Geophysical Research Letters

RESEARCH LETTER
10.1029/2022GL102494

On the Lateral Entrainment Instability in the Inner Core Region of Tropical Cyclones

Ping Zhu[1], Jun A. Zhang[2,3], and Frank D. Marks[3]

[1]Department of Earth and Environment, Florida International University, Miami, FL, USA, [2]Cooperative Institute for Marine and Atmospheric Studies, University of Miami, Miami, FL, USA, [3]Hurricane Research Division, Atlantic Oceanographic and Meteorological Laboratory, NOAA, Miami, FL, USA

Key Points:

- Lateral entrainment of air from the moat region into eyewall and rainbands of a tropical cyclone (TC) satisfies the instability criterion
- Positive buoyancy flux induced by the entrainment is an important source of turbulent kinetic energy for the eyewall and rainband clouds
- Lateral entrainment instability should be included in turbulent mixing parameterizations in TC forecast models

Supporting Information:

Supporting Information may be found in the online version of this article.

Correspondence to:

P. Zhu,
zhup@fiu.edu

Citation:

Zhu, P., Zhang, J. A., & Marks, F. D. (2023). On the lateral entrainment instability in the inner core region of tropical cyclones. *Geophysical Research Letters*, *50*, e2022GL102494. https://doi.org/10.1029/2022GL102494

Received 9 DEC 2022
Accepted 23 MAR 2023

Author Contributions:

Conceptualization: Ping Zhu
Data curation: Ping Zhu, Jun A. Zhang, Frank D. Marks
Formal analysis: Ping Zhu
Funding acquisition: Ping Zhu
Investigation: Ping Zhu
Methodology: Ping Zhu
Project Administration: Ping Zhu
Resources: Ping Zhu, Jun A. Zhang, Frank D. Marks
Software: Ping Zhu
Supervision: Ping Zhu
Validation: Ping Zhu, Jun A. Zhang
Visualization: Ping Zhu
Writing – original draft: Ping Zhu

Abstract Entrainment of dry moat air with low equivalent potential temperature laterally into the eyewall and rainbands is a unique turbulent process in the inner-core region of a tropical cyclone (TC). By analyzing in-situ aircraft measurements collected by the reconnaissance flights that penetrated the eyewalls and rainbands of Hurricanes Rita (2005), Patricia (2015), Harvey (2017), and Michael (2018), as well as numerical simulations of Hurricanes Patricia (2015), and Michael (2018), we show that the moat air entrained into the eyewall and rainbands meets the instability criterion, and therefore, sinks unstably as a convective downdraft. The resultant positive buoyancy fluxes are an important source for the turbulent kinetic energy (TKE) in the eyewall and rainband clouds. This mechanism of TKE generation via lateral entrainment instability should be included in the TKE-type turbulent mixing schemes for a better representation of turbulent transport processes in numerical forecasts of TCs.

Plain Language Summary Turbulence is commonly regarded as a chaotic flow feature pertaining to the planetary boundary layer (PBL). In the inner core of a tropical cyclone (TC), however, turbulence can also be generated in the eyewall and rainbands above the PBL by cloud processes. The turbulence at the edge of the eyewall/rainbands not only experiences the large lateral thermodynamic contrasts across the interface between clouds and moat but also entrains moat air into clouds. Previous studies suggest that under certain conditions the entrained air into the clouds can sink unstably as convective downdrafts, leading to the generation of turbulent kinetic energy (TKE) in the clouds. By analyzing in-situ aircraft measurements collected during the reconnaissance flights that penetrated the eyewalls and rainbands of Hurricanes Rita (2005), Patricia (2015), Harvey (2017), and Michael (2018), as well as numerical simulations of Patricia (2015) and Michael (2018), this study shows that the moat air entrained into the eyewall and rainbands meets the instability criterion. An estimate of the entrainment buoyancy fluxes suggests that the lateral entrainment instability is an important source of TKE in the eyewall and rainbands, and thus, it needs to be included in the TKE-type turbulence schemes used in numerical forecasts of TCs.

1. Introduction

The entrainment instability at the top of clouds was first recognized by Lilly (1968) and later well documented by Deardorff (1980) and Randall (1980). Under cloud free conditions, entrainment of air from the free atmosphere above into the turbulent boundary layer tends to destroy the turbulent kinetic energy (TKE) since the buoyancy force acts to oppose the vertical motions in the boundary layer. For the boundary layer topped by stratocumulus clouds, however, the evaporative cooling of the unsaturated free atmosphere air that has been entrained into clouds may cause the entrained air to sink unstably as a convective downdraft owing to its negative buoyancy. This process leads to the generation of TKE in the stratocumulus layer. Deardorff (1980) showed that the entrainment buoyancy flux, $\left(\overline{w'\theta'_v}\right)_{ctp\_e}$, may be written as a function of the jumps of conserved thermodynamic variables across the top of the stratocumulus layer as,

$$\left(\overline{w'\theta'_v}\right)_{ctp\_e} = w_{ctp\_e}\left(-\alpha\Delta_{ctp}\theta_e + \overline{\theta}\Delta_{ctp}q_t\right), \tag{1}$$

where θ_e is the equivalent potential temperature defined as $\theta_e = \theta\left(1 + \frac{L}{c_pT}q\right)$ in the unit of Kelvin (K); T is the temperature (K); θ is the potential temperature (K); q is the water vapor mixing ratio (kg/kg); $L = 2.5 \times 10^6$ (J/kg) is the specific latent heat of vapourization; $c_p = 1{,}005$ (J/kg · K) is the specific heat of dry air at the constant

Writing – review & editing: Ping Zhu, Jun A. Zhang, Frank D. Marks

pressure; q_t is the total water mixing ratio (kg/kg); θ_v is the virtual potential temperature (K); w_{ctp_e} is the cloud-top entrainment velocity (m/s); α is a unitless theoretical coefficient resulting from the derivation involving with the moist thermodynamics, and it has a value near 0.5, but may vary from 1/3 to 2/3 depending on specific conditions; Δ_{ctp} is defined as the difference of the above-cloud value minus the in-cloud value; and overbar and prime indicate the mean and perturbations away from the mean, respectively. Since w_{ctp_e} is positive and $\Delta_{ctp} q_t$ is negative, if $\Delta_{ctp}\theta_e$ is more negative than a criterion, $\Delta_{ctp}\theta_e < (\Delta_{ctp}\theta_e)_{\text{crit}} = \overline{\theta}\Delta_{ctp} q_t/\alpha$, it will, then, result in positive entrainment buoyancy fluxes, $\left(\overline{w'\theta'_v}\right)_{ctp\_e} > 0$, leading to the generation of TKE in the stratocumulus layer. This is known as the cloud top entrainment instability and has been identified as an important mechanism for generating TKE in the clouds to maintain the stratocumulus layer.

Unlike the shallow-cloud topped boundary layer that is cleanly separated from the dry free atmosphere above by a capping inversion, observations show that in the eyewall and rainbands of a tropical cyclone (TC) large TKEs extend all the way to the upper troposphere from the boundary layer (e.g., Lorsolo et al., 2010; Marks et al., 2008; Zhang & Montgomery, 2012; Zhu et al., 2019) with no physical interface, such as an inversion, separating the turbulence generated by boundary layer processes and cloud processes aloft. Thus, cloud top entrainment instability associated with the shallow stratocumulus does not exist or is negligible in the TC inner-core region. However, turbulence generated in the eyewall and rainbands experiences a large lateral thermodynamic contrast across the interface between the eyewall/rainbands and moat. As an illustration, Figure 1 shows a height-radius distribution of the simulated total water mixing ratio and velocity vectors at the outer edge of the eyewall from a large eddy simulation (LES) of Hurricane Isabel (2003) by Y. B. Li et al. (2022). There are two well-defined large overturning eddy circulations in the scene. One is in the boundary layer and the other is in the mid troposphere at the cloud edge indicated by the thick black arrows. In both cases, turbulent eddies not only experience drastic lateral contrasts across the edge of the eyewall, but also entrain the dry and low θ_e air from the moat region laterally into the eyewall. Following the entrainment instability requirement (Deardorff, 1980), if the lateral entrainment of the low θ_e moat air into the eyewall or rainbands meets the instability criterion, that is,

$$\Delta_{\text{lat}}\theta_e < (\Delta_{\text{lat}}\theta_e)_{\text{crit}} = \overline{\theta}\Delta_{\text{lat}} q_t/\alpha, \tag{2}$$

where Δ_{lat} refers to the lateral difference of the moat-air value minus the in-cloud value, then, lateral entrainment instability can occur, resulting in positive lateral entrainment buoyancy fluxes. This positive buoyancy flux can in turn serve as an important source for TKE generation in the eyewall and rainbands via buoyancy production of TKE (Stull, 1988).

Therefore, the main objective of this study is to verify if the lateral entrainment in the TC inner-core region satisfies the instability criterion stated above using both observations and numerical simulations. Based on the results, the importance and potential application of this TKE generation mechanism in eyewall and rainband clouds via lateral entrainment instability to the TKE type of turbulent mixing parameterizations used in TC forecast models are further discussed.

2. Evidences of Lateral Entrainment Instability in TC Inner Core

To evaluate if the moat air laterally entrained into the eyewall and rainband clouds meets the instability criterion and is able to sink unstably as a convective downdraft, we examined the in-situ aircraft data collected during the Hurricane Research Division (HRD) reconnaissance flights that penetrated the eyewall and rainbands of Hurricanes Rita (2005), Patricia (2015), Harvey (2017), and Michael (2018) in total 113 radial legs. As an illustration, Figure 2 shows the 8 flight routes into Michael (2018) and the radial profiles of relative humidity, water vapor mixing ratio, equivalent potential temperature θ_e, and wind speed as a function of the distance from the storm center (i.e., radius) at approximately 750 hPa altitude from one of these legs that penetrated into Michael (2018). Details of the radial leg data from the HRD reconnaissance flights are provided in the Section S1 of Supporting Information S1. Since the flights do not have cloud measurements, we infer the locations of eyewall and rainbands as the radii where relative humidities are close to or exceed 1 as shown in Figure 2b. We tested several values of relative humidity for saturation from 93% to 100%. It only shows a marginal effect on the analysis results. Therefore, in this paper the eyewall and rainbands in the radial legs are identified wherever the relative humidity exceeds 94%. The eyewall is, then, defined to be the region closest to the maximum wind speed (Figure 2e). The radial profile shown in Figure 2d clearly shows that the moat air in-between eyewall and rainbands has a lower θ_e than the saturated air in the eyewall and rainbands.

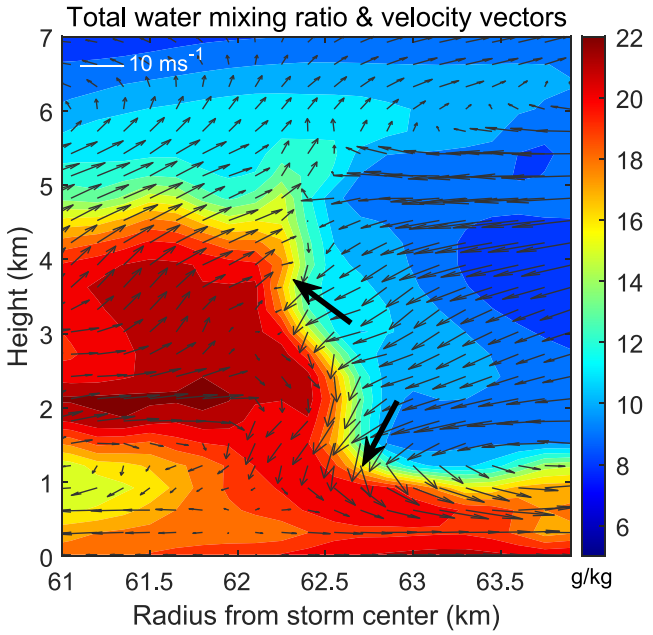

Figure 1. Height-radius distribution of total water mixing ratio (shading, *g*/kg) overlapped with the wind vectors associated with vertical velocity and radial flow near the outer edge of the eyewall from a large eddy simulation of Hurricane Isabel (2003) documented by Y. B. Li et al. (2022). To clearly show the overturning eddy circulations, the mean radial flow over the area has been removed. Two thick dark arrows indicate the overturning turbulent eddy circulations in the scene.

We then estimate the difference of θ_e and mixing ratio between the identified unsaturated moat region and saturated eyewall and rainbands as follows. Since the radial resolution of the flight data is ~100–150 m, we average 20 observation points (~2–3 km) just inside and outside of the identified eyewall and rainbands to represent the mean thermodynamic properties of cloudy and moat air involved in the lateral entrainment, and then, calculate their differences between the moat as well as saturated eyewall and rainbands to examine if the entrained moat air into the eyewall and rainbands meets the instability criterion. Figure 3 shows the estimated $\Delta\theta_e$ against the instability criterion $\overline{\theta}\Delta q/\alpha$ for all edges between the identified eyewalls/rainbands and moats of the 50 radial flight legs into Rita (2005), 7 legs into Patricia (2015), 22 legs into Harvey (2017), and 34 legs into Michael (2018). Most of the estimates fall clearly in the unstable regime with only a few points falling in the stable regime. The possible reason for these points not to satisfy the instability criterion is explored and is provided in the Section S3.1 of Supporting Information S1.

It should be pointed out that due to the lack of hydrometeor measurements in the aircraft data we have to replace the total water mixing ratio with the water vapor mixing ratio when calculating the instability criterion. Therefore, the actual value of $\overline{\theta}\Delta q/\alpha$ should be slightly more negative if the total water mixing ratio q_t were used. However, even if the hydrometeor mixing ratios were available and included in the calculation, the majority of the data points should still fall in the unstable regime, indicating that the moat air that is entrained laterally into eyewall and rainband clouds has sufficiently low θ_e to meet the instability criterion and sinks unstably due to its own negative buoyancy. It should also be noted that the above analysis only shows an entrainment instability potential. It remains unknown what percentage of moat air is

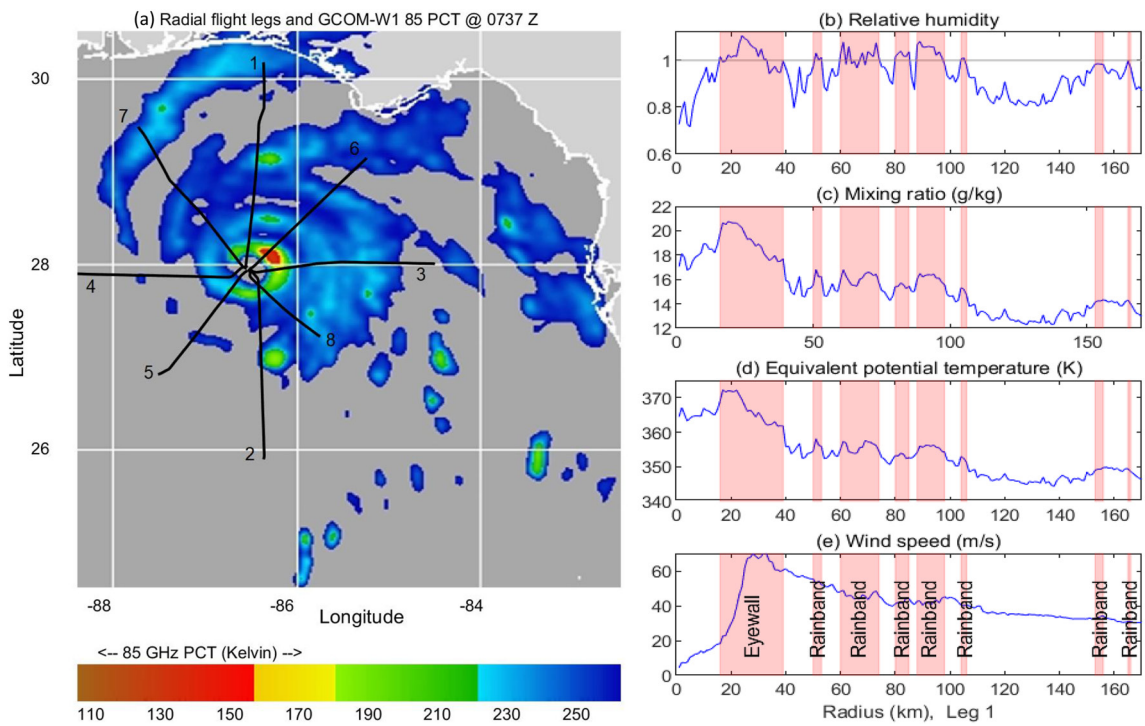

Figure 2. (a): Selected flights that penetrated into the eyewall and rainbands of Hurricane Michael (2018). (b)–(e): Radial profiles of relative humidity, water vapor mixing ratio, equivalent potential temperature, and wind speed as a function of radii from the storm center at ~750 hPa respectively from one of the flight legs.

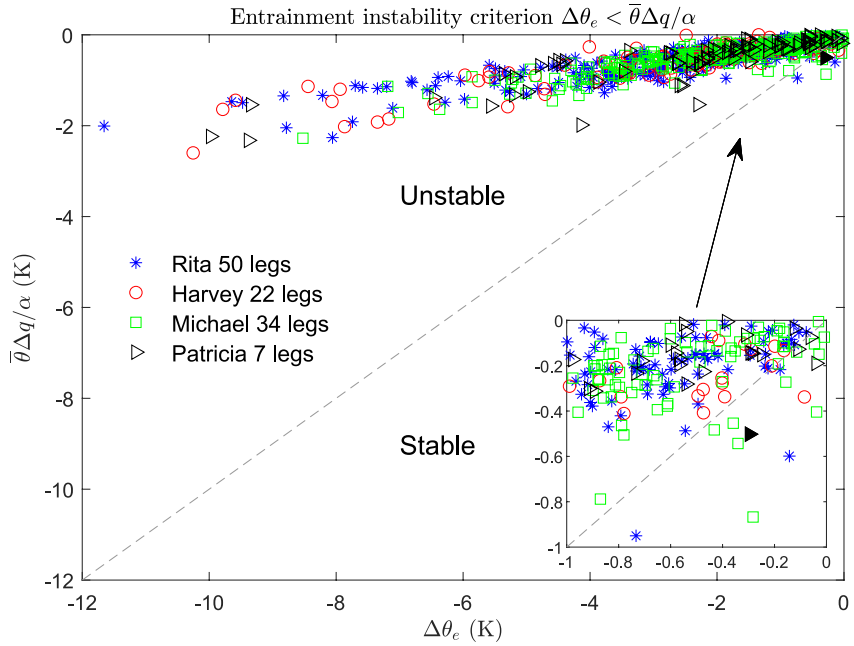

Figure 3. Equivalent potential temperature jumps across the identified eyewall/rainbands and moat, $\Delta\theta_e$, as a function of the corresponding instability criterion $\overline{\theta}\Delta q/\alpha$ for 50 flight legs into Rita (2005), 7 legs into Patricia (2015), 22 legs into Harvey (2017), and 34 legs into Michael (2018) where Δ is defined as the difference of moat-air value minus in-cloud value. The

actually entrained into the eyewall and rainband clouds by turbulence. This issue needs to be further investigated using relevant high-resolution observations and LESs.

To further evaluate the lateral entrainment instability in the TC inner core, we examined the numerical simulations of Hurricane Michael (2018) by the global-nested version of Hurricane Analysis and Forecast System (HAFS-globalnest, Zhu et al., 2021) and Hurricane Patricia (2015) by the Hurricane Weather Research and Forecasting (HWRF) model version 3.9a. Details of the numerical simulations are provided in the Section S2 of Supporting Information S1. Figures 4a and 4b show two arbitrary snapshots of cloud hydrometeor mixing ratio from the HAFS simulation of Michael (2018) and HWRF simulation of Patricia (2015) during their rapid intensification (RI) periods. Three consecutive grid points just inside, at, and outside of the outer edge of the eyewall are randomly selected whose locations with respect to the eyewall are shown in the inlaid panels, respectively. The distance between the grid points is approximately 1.22 km for HWRF since it was configured at the grid resolution of 0.011°, and 3 km for HAFS. The entrainment instability across the edge of the eyewall is, then, evaluated by calculating the instability parameter $\Delta_{\text{lat}}\theta_e - \overline{\theta}\Delta_{\text{lat}}q_t/\alpha$ using various combinations of the differences between the three grid points: green minus black, red minus green, and red minus black, respectively. The results (Figures 4c and 4d) clearly show that $\Delta_{\text{lat}}\theta_e$ is more negative than the instability criterion $\overline{\theta}\Delta_{\text{lat}}q_t/\alpha$ throughout almost the entire vertical column in both simulations, indicating that the entrained low θ_e moat air into the eyewall meets the instability criterion and thus will sink spontaneously due to its own negative buoyancy to generate TKE in the eyewall. One exception is the shallow layer in-between 1 and 2 km where the instability parameter $\Delta_{\text{lat}}\theta_e - \overline{\theta}\Delta_{\text{lat}}q_t/\alpha$ appears to be positive. Our analysis shows that the stable lateral entrainment in this shallow layer is likely caused by the subsidence warming outside the clouds so that the entrained moat air into the eyewall there does not have sufficiently low θ_e to sink unstably. The detailed analyses on this issue are provided in the Section S3.2 of Supporting Information S1.

We have also examined the lateral entrainment instability criterion at various locations along the outer edge of the eyewall with respect to down/up wind shear. The results are similar to what is shown in Figures 4c and 4d. However, dynamically it remains unknown which quadrant of the eyewall with respect to wind shear is preferred for lateral entrainment. This issue needs to be further investigated.

To further examine the robustness of lateral entrainment instability of entraining the moat air into the eyewall, we conducted the axisymmetric analysis. Figures 4e–4h show the azimuthal-mean pseudo eyewall hydrometeor

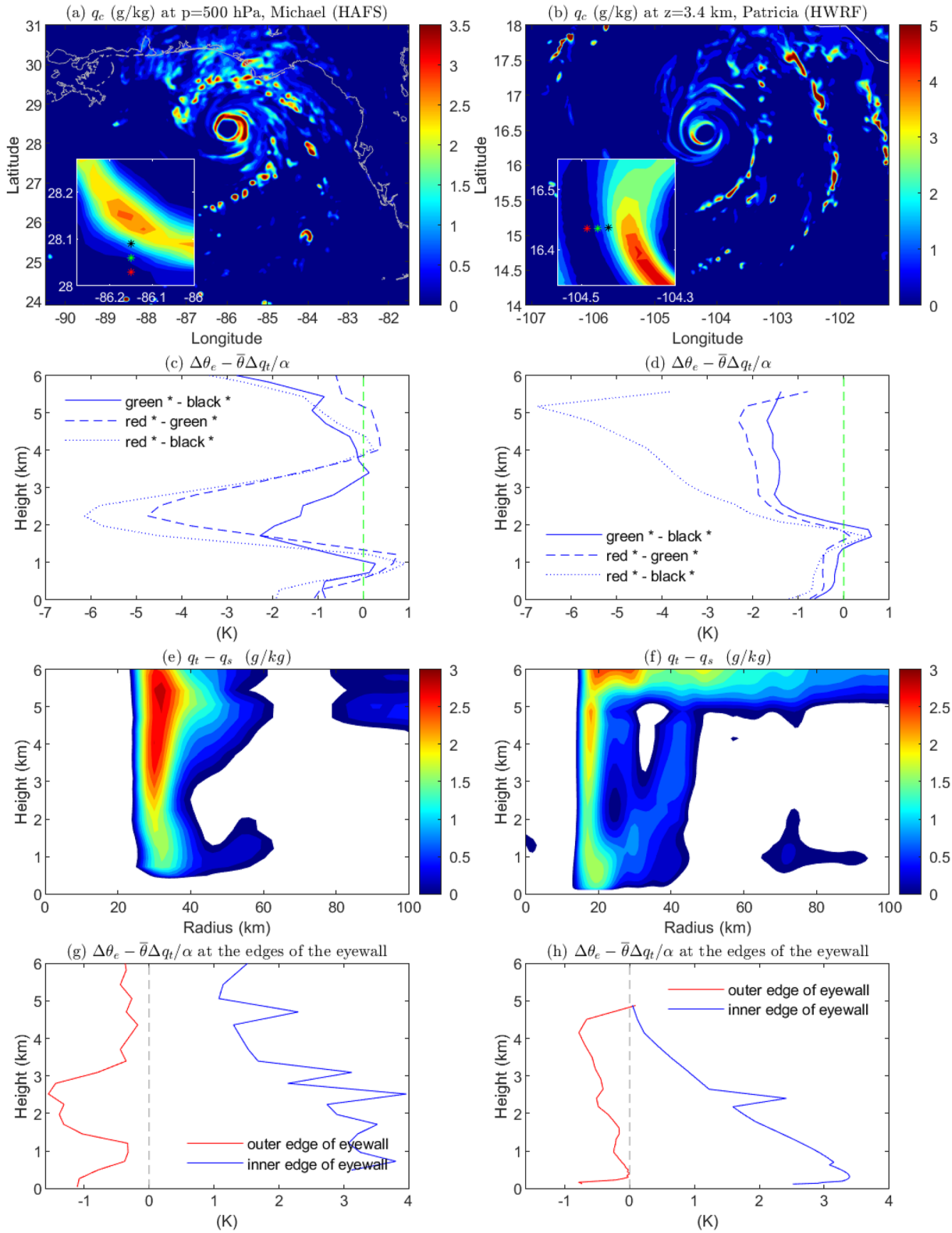

Figure 4. (a) and (b) Hydrometeor mixing ratio at the altitude of 500 hPa and 3.4 km at an arbitrary time during the rapid intensification of Michael (2018) and Patricia (2015) simulated by HAFS and Hurricane Weather Research and Forecasting, respectively. The inlaid panel shows the zoom-in view of the eyewall. Red, green, and black stars indicate the grid points in the vicinity of the eyewall to be analyzed. (c) and (d): Instability parameter $\Delta\theta_e - \overline{\theta}\Delta q/\alpha$ calculated using the different jumps among red, green, and black grid points, respectively. (e) and (f): Radius-height structure of azimuthal-mean cloud condensate defined as $q_t - q_s$ (g/kg) of Michael (2018) and Patricia (2015). (g) and (h): Vertical profiles of instability parameter $\Delta\theta_e - \overline{\theta}\Delta q/\alpha$ at the inner and outer edges of the eyewall.

mixing radio and vertical profiles of instability parameter $\Delta_{\text{lat}}\theta_e - \overline{\theta}\Delta_{\text{lat}}q_t/\alpha$ at the inner and outer edges of the azimuthal-mean eyewall. Note that we did not use the azimuthal-mean hydrometeor mixing ratio simulated directly by the models to define the clouds. This is because the eyewall and rainbands of a TC always deviate away from axisymmetry to certain degrees. Thus, when performing azimuthal average, it may generate false saturation at certain radii in the height-radius space. For example, assuming that an asymmetric convection occurs at a location, say, 30 km in radius away from the storm center, and there is no convection elsewhere along this radius. An azimuthal-mean calculation will average the hydrometeors of this asymmetric convection over the entire radius of 30 km. To prevent this false saturation in the height-radius space, here we define saturation wherever the azimuthal-mean of the simulated total water mixing ratio $\overline{q}_t$ is greater than the saturated mixing ratio $\overline{q}_s$ determined by the azimuthal-mean temperature from the simulations.

We, then, estimate the entrainment instability parameter $\Delta_{\text{lat}}\overline{\theta}_e - \overline{\theta}\Delta_{\text{lat}}\overline{q}_t/\alpha$ at the inner and outer edges of the eyewall using $\overline{q}_t$ and $\overline{\theta}_e$ just inside and outside the eyewall (4 km from the defined cloud edge). The results are shown in Figures 4g and 4h. It clearly shows that the lateral entrainment at the outer edge of the eyewall robustly meets the instability criterion. However, the lateral entrainment at the inner edge of the eyewall fails to satisfy the instability criterion. The likely reason is that a TC has a warm core. The high temperature in a TC's eye causes $\Delta\overline{\theta}_e$ to be less negative than $\frac{\overline{\theta}}{\alpha}\Delta\overline{q}_t$. It should be kept in mind, however, that the actual lateral entrainment does not entrain the mean properties of moat air into the mean state of the eyewall or rainbands, rather, it occurs locally. Therefore, the estimated instabilities using the mean properties shown in Figures 4g and 4h do not represent the real lateral entrainment in the TC inner core.

3. Conclusion and Discussion

Airborne radar observations show that large TKEs are generated in the eyewalls and rainbands by cloud processes aloft (e.g., Lorsolo et al., 2010; Marks et al., 2008; Zhang & Montgomery, 2012; Zhu et al., 2019). The resultant turbulent transport above the boundary layer plays an important role in the intensification of TCs (Zhu et al., 2019, 2021). In this study, by analyzing the in-situ aircraft data collected during the reconnaissance flights that penetrated the eyewall and rainbands of Hurricanes Rita (2005), Patricia (2015), Harvey (2017), and Michael (2018), as well as numerical simulations of Michael (2018) by HAFS and Patricia (2015) by HWRF, we show that the moat air if entrained into the eyewalls and rainbands will meet the instability criterion, leading to the potential unstable convective downdraft. The importance of this mechanism of TKE generation in the eyewall and rainbands via lateral entrainment instability may be inferred from an estimation of the resultant entrainment buoyancy fluxes. Following Equation (1), the buoyancy fluxes induced by the lateral entrainment of moat air into the eyewalls and rainbands may be written as, $\rho c_p v_{\text{lat}}\left(-\alpha\Delta_{\text{lat}}\theta_e + \overline{\theta}\Delta_{\text{lat}}q_t\right)$, where ρ is the air density and v_{lat} is the lateral entrainment velocity. Although to date we have little knowledge on the lateral entrainment velocity in the TC inner core between the moat and convection, a lateral entrainment velocity of 0.3 m/s for the entrainment into convective thermals was previously derived from the comprehensive lidar and aircraft measurements (Crum et al., 1987). Based on the in-situ aircraft measurements (Figure 3) and numerical simulations (Figures 4c and 4d), it is reasonable to assume the thermodynamic jump across the edge of eyewall and rainband clouds to be in a range $-\alpha\Delta_{\text{lat}}\theta_e + \overline{\theta}\Delta_{lat}q_t \propto [1-4]$K, further taking $v_{\text{lat}} = [0.1\text{–}0.4]$ m/s based on the available observations (Crum et al., 1987), then, the entrainment buoyancy fluxes would be in a range of 100–1600 w/m^2, suggesting that the lateral entrainment instability should be one of the important mechanisms for generating TKEs in the eyewall and rainband clouds via TKE buoyancy production (Stull, 1988).

The TKE-type turbulent mixing schemes now have been widely adopted in many research and operational models used for predicting TCs, such as, the Eddy-Diffusivity-Mass-Flux (EDMF) TKE scheme (Han & Bretherton, 2019) used in the HAFS, a multi-scale Unified Forecast System operational model and data assimilation package capable of providing analyses and forecasts of track, intensity, and inner core structure of TCs out to 7 days. The TKE schemes are attractive because they can provide a representation of turbulent transport induced by both the boundary-layer processes and cloud processes aloft in a unified manner regardless of the boundary layer height, provided that the buoyancy production, shear production, transport, and dissipation of TKE in a TKE budget equation can be correctly determined. This feature of a TKE scheme is particularly important in the TC inner core since the boundary layer becomes ill-defined as air approaches the eyewall and is pulled up into the active convection (Shapiro, 1983; Smith et al., 2008; Smith & Montgomery, 2010; Zhang et al., 2011). In the

eyewalls and rainbands, buoyancy production is an important source of TKE generation. The result presented in this study indicates that the lateral entrainment instability is an important physical process that needs to be included in the calculation of buoyancy production of TKE in numerical forecasts of TCs. Moreover, the lateral entrainment of moat air into the convective eyewalls and rainbands is a process that links horizontal and vertical turbulent mixing in the TC inner core. The positive lateral entrainment buoyancy flux promotes the TKE generation in the eyewall, which ensue enhances the lateral entrainment instability as more low-θ_e air in the moat is entrained into the eyewall. This positive feedback between the TKE generation in the eyewall clouds and lateral entrainment instability is unique for turbulence development and transport in the TC inner-core region, and thus, it must be represented realistically in numerical models for predicting TCs. We believe that the inclusion of lateral entrainment instability in model turbulent mixing schemes could address some of the issues regarding turbulence parameterization in TC simulations and correct prediction of RI raised by some recent students (e.g., X. Li & Pu, 2021; Lu & Wang, 2019). To appropriately include lateral entrainment process in models, future researches are recommended to focus on investigating the dynamic aspect that determines the actual fraction of the moat air entrained into the eyewall and rainbands, quantifying the lateral entrainment velocity using observations and large-eddy simulations, and developing appropriate methods to explicitly include lateral entrainment buoyancy fluxes in the calculation of the buoyancy production of TKE in the TKE-based turbulent mixing schemes.

Data Availability Statement

Aircraft data, numerical simulation data, and Matlab codes for analyzing data used in this study can be accessed at http://vortex.ihrc.fiu.edu/download/Entrainment/.

Acknowledgments
This work is supported by NOAA/HFIP under the Grant NA18NWS4680057, NOAA/JTTI under the Grant NA22OAR4590177, and National Science Foundation under the Grants 2211307 and 2211308. We are very grateful to the two anonymous reviewers for their constructive and insightful comments, which lead to the improvement of the paper.

References

Crum, T. D., Stull, R. B., & Eloranta, E. W. (1987). Coincident lidar and aircraft observations of entrainment into thermals and mixed layers. *Journal of Climate and Applied Meteorology*, *26*(7), 774–788. https://doi.org/10.1175/1520-0450(1987)026<0774:CLAAOO>2.0.CO;2

Deardorff, J. W. (1980). Cloud top entrainment instability. *Journal of the Atmospheric Sciences*, *37*(1), 131–147. https://doi.org/10.1175/1520-0469(1980)037<0131:CTEI>2.0.CO;2

Han, J., & Bretherton, C. S. (2019). TKE-based moist eddy-diffusivity mass-flux (EDMF) parameterization for vertical turbulent mixing. *Weather and Forecasting*, *34*(4), 869–886. https://doi.org/10.1175/WAF-D-18-0146.1

Li, X., & Pu, Z. (2021). Vertical eddy diffusivity parameterization based on a large-eddy simulation and its impact on prediction of hurricane landfall. *Geophysical Research Letters*, *48*(2), e2020GL090703. https://doi.org/10.1029/2020GL090703

Li, Y. B., Zhu, P., Gao, Z. Q., & Cheung, K. (2022). Sensitivity of large eddy simulations of tropical cyclone to sub-grid scale mixing parameterization. *Atmospheric Research*, *265*, 105922. https://doi.org/10.1016/j.atmosres.2021

Lilly, D. K. (1968). Models of cloud-topped mixed layer under a strong inversion. *Quarterly Journal of the Royal Meteorological Society*, *94*(401), 292–837. https://doi.org/10.1002/qj.49709440106

Lorsolo, S., Zhang, J. A., Marks, F. D., & Gamache, J. (2010). Estimation and mapping of hurricane turbulent energy using airborne Doppler measurements. *Monthly Weather Review*, *138*(9), 3656–3670. https://doi.org/10.1175/2010MWR3183.1

Lu, X., & Wang, X. G. (2019). Improving hurricane analyses and predictions with TCI, IFEX field campaign observations, and CIMSS AMVs using the advanced hybrid data assimilation system for HWRF. Part I: What is missing to capture the rapid intensification of Hurricane Patricia (2015) when HWRF is already initialized with a more realistic analysis? *Monthly Weather Review*, *147*(4), 1351–1370. https://doi.org/10.1175/MWR-D-18-0202.1

Marks, F. D., Black, P. G., Montgomery, M. T., & Burpee, R. W. (2008). Structure of the eye and eyewall of Hurricane Hugo (1989). *Monthly Weather Review*, *136*(4), 1237–1259. https://doi.org/10.1175/2007MWR2073.1

Randall, D. A. (1980). Conditional instability of the first kind upside down. *Journal of the Atmospheric Sciences*, *37*(1), 125–130. https://doi.org/10.1175/1520-0469(1980)037<0125:CIOTFK>2.0.CO;2

Shapiro, L. (1983). The asymmetric boundary-layer flow under a translating hurricane. *Journal of the Atmospheric Sciences*, *40*(8), 1984–1998. https://doi.org/10.1175/1520-0469(1983)040<1984:TABLFU>2.0.CO;2

Smith, R. K., & Montgomery, M. T. (2010). Hurricane boundary layer theory. *Quarterly Journal of the Royal Meteorological Society*, *136*(652), 1665–1670. https://doi.org/10.1002/qj.679

Smith, R. K., Montgomery, M. T., & Vogl, S. (2008). A critique of Emanuel's hurricane model and potential intensity theory. *Quarterly Journal of the Royal Meteorological Society*, *134*(632), 551–561. https://doi.org/10.1002/qj.241

Stull, R. B. (1988). *An introduction to boundary-layer meteorology* (670pp). Kluwer.

Zhang, J. A., Marks, F. D., Montgomery, M. T., & Lorsolo, S. (2011). An estimation of turbulent characteristics in the low-level region of intense Hurricanes Allen (1980) and Hugo (1989). *Monthly Weather Review*, *139*(5), 1447–1462. https://doi.org/10.1175/2010MWR3435.1

Zhang, J. A., & Montgomery, M. T. (2012). Observational estimates of the horizontal eddy diffusivity and mixing length in the low-level region of intense hurricanes. *Journal of the Atmospheric Sciences*, *69*(4), 1306–1316. https://doi.org/10.1175/JAS-D-11-0180.1

Zhu, P., Hazelton, A., Zhang, Z., Marks, D. F., & Tallapragada, V. (2021). The role of eyewall turbulent transport in the pathway to intensification of tropical cyclones. *Journal of Geophysical Research: Atmospheres*, *126*(17), e2021JD034983. https://doi.org/10.1029/2021JD034983

Zhu, P., Tyner, B., Zhang, J. A., Aligo, E., Gopalakrishnan, S., Marks, F. D., et al. (2019). Role of eyewall and rainband in-cloud turbulent mixing in tropical cyclone intensification. *Atmospheric Chemistry and Physics*, *19*(22), 14289–14310. https://doi.org/10.5194/acp-19-14289-2019

References From the Supporting Information

Aligo, E. A., Ferrier, B., & Carley, J. R. (2018). Modified NAM microphysics for forecasts of deep convective storms. *Monthly Weather Review*, *146*(12), 4115–4153. https://doi.org/10.1175/MWR-D-17-0277.1

Chen, J.-H., & Lin, S.-J. (2013). Seasonal predictions of tropical cyclones using a 25-km-resolution general circulation model. *Journal of Climate*, *26*(2), 380–398. https://doi.org/10.1175/JCLI-D-12-00061.1

French, J. F., Drennan, W. M., Zhang, J. A., & Black, P. G. (2007). Turbulent fluxes in the hurricane boundary layer, Part I: Momentum flux. *Journal of the Atmospheric Sciences*, *64*(4), 1089–1102. https://doi.org/10.1175/JAS3887.1

Han, J., Witek, M., Teixeira, J., Sun, R., Pan, H.-L., Fletcher, J. K., & Bretherton, C. S. (2016). Implementation in the NCEP GFS of a hybrid eddy-diffusivity mass-flux (EDMF) boundary layer parameterization with dissipative heating and modified stable boundary layer mixing. *Weather and Forecasting*, *31*(1), 341–352. https://doi.org/10.1175/WAF-D-15-0053.1

Han, J., Wang, W., Kwon, Y. C., Hong, S., Tallapragada, V., & Yang, F. (2017). Updates in the NCEP GFS cumulus convection schemes with scale and aerosol Awareness. *Weather and Forecasting*, *32*(5), 2005–2017. https://doi.org/10.1175/WAF-D-17-0046.1

Harris, L. M., & Lin, S.-J. (2013). A two-way nested global-regional dynamical core on the cubed-sphere grid. *Monthly Weather Review*, *141*(1), 283–306. https://doi.org/10.1175/MWR-D-11-00201.1

Hazelton, A. T., Zhang, Z., Liu, B., Dong, J., Alaka, G., Wang, W., et al. (2021). 2019 Atlantic hurricane forecasts from the Global-Nested Hurricane Analysis and Forecast System (HAFS): Composite statistics and key events. *Weather and Forecasting*, *36*(2), 519–538. https://doi.org/10.1175/WAF-D-20-0044.1

Hong, S.-Y., & Pan, H.-L. (1996). Nonlocal boundary layer vertical diffusion in a Medium-Range Forecast model. *Monthly Weather Review*, *124*(10), 2322–2339. https://doi.org/10.1175/1520-0493(1996)124<2322:NBLVDI>2.0.CO;2

Iacono, M. J., Delamere, J. S., Mlawer, E. J., Shephard, M. W., Clough, S. A., & Collins, W. D. (2008). Radiative forcing by long-lived greenhouse gases: Calculations with the AER radiative transfer models. *Journal of Geophysical Research*, *113*(D13), D13103. https://doi.org/10.1029/2008JD009944

Khelif, D., Burns, S. P., & Friehe, C. A. (1999). Improved wind measurements on research aircraft. *Journal of Atmospheric and Oceanic Technology*, *16*(7), 860–875. https://doi.org/10.1175/1520-0426(1999)016<0860:IWMORA>2.0.CO;2

Lenschow, D. H. (1986). Aircraft measurements in the boundary layer. In *Probing the atmospheric boundary layer* (pp. 39–55). American Meteorological Society.

Lin, S.-J. (2004). A "vertically Lagrangian" finite-volume dynamical core for global models. *Monthly Weather Review*, *132*(10), 2293–2307. https://doi.org/10.1175/1520-0493(2004)132<2293:avlfdc>2.0.co;2

Willoughby, H. E., & Chelmow, M. (1982). Objective determination of hurricane tracks from aircraft observations. *Monthly Weather Review*, *110*(9), 1298–1305. https://doi.org/10.1175/1520-0493(1982)110<1298:ODOHTF>2.0.CO;2